



HAL
open science

Mapping grassland plant communities using a fuzzy approach to address floristic and spectral uncertainty

Sébastien Rapinel, Nicolas Rossignol, Laurence Hubert-Moy, Jan-Bernard Bouzillé, Anne Bonis

► **To cite this version:**

Sébastien Rapinel, Nicolas Rossignol, Laurence Hubert-Moy, Jan-Bernard Bouzillé, Anne Bonis. Mapping grassland plant communities using a fuzzy approach to address floristic and spectral uncertainty. *Applied Vegetation Science*, 2018, 21 (4), pp.678-693. 10.1111/avsc.12396 . hal-01937631

HAL Id: hal-01937631

<https://univ-rennes.hal.science/hal-01937631>

Submitted on 17 Dec 2020

HAL is a multi-disciplinary open access archive for the deposit and dissemination of scientific research documents, whether they are published or not. The documents may come from teaching and research institutions in France or abroad, or from public or private research centers.

L'archive ouverte pluridisciplinaire **HAL**, est destinée au dépôt et à la diffusion de documents scientifiques de niveau recherche, publiés ou non, émanant des établissements d'enseignement et de recherche français ou étrangers, des laboratoires publics ou privés.

1 Research article

2 **Title:** Mapping grassland plant communities using a fuzzy approach to address floristic and
3 spectral uncertainty

4 **Author names and addresses:**

5 Rapinel, S. (corresponding author, sebastien.rapinel@univ-rennes2.fr) ^{1,2}

6 Rossignol, N. (nicolas.rossignol@univ-rennes1.fr) ¹

7 Hubert-Moy, L. (laurence.moy@univ-rennes2.fr) ²

8 Bouzillé, J.B. (jan-bernard.bouzille@univ-rennes1.fr) ¹

9 Bonis, A. (anne.bonis@univ-rennes1.fr) ^{1(a)}

10 ¹ CNRS UMR 6553 ECOBIO, Université Rennes 1, Avenue Général Leclerc, 35000 Rennes,
11 France

12 ^(a) Present address: GEOLAB, UMR 6042 CNRS-UCA 4, rue Ledru 63000 Clermont-Ferrand,
13 France, anne.bonis@uca.fr

14 ² CNRS UMR 6554 LETG, Université Rennes 2, Place du Recteur Henri Le Moal, 35000
15 Rennes, France

16 **Printed journal page estimate:** 10680 words (13.0 pages), tables 1.0 pages, figures 2.0
17 pages, total 16.0 pages.

18

19

20 **Abstract:**

21 **Aims:** The mapping and monitoring of natural vegetation is a challenging but important
22 objective for environmental management. Although remote sensing has been used to map
23 plant communities for several years, the maps produced are not sufficiently accurate to meet
24 management requirements. This can be explained by the cumulative effects of floristic and
25 spectral uncertainty. The objective of this study was to accurately map grassland plant
26 communities using a comprehensive fuzzy approach in order to address floristic and spectral
27 uncertainty.

28 **Location:** Sub-brackish wet grasslands, Marais Poitevin, France.

29 **Methods:** We first created a compromise typology - floristically and spectrally consistent - to
30 perform fuzzy noise clustering on a joint PCA matrix derived from vegetation *relevés* and
31 remote sensing data. This typology had two levels, which corresponded to spectral signatures
32 and plant communities, respectively. Second, we mapped grassland plant communities to
33 predict the fuzzy model from the remote sensing data. We applied this approach using 1- a
34 very high spatial resolution multispectral satellite image and a LiDAR-derived Digital Terrain
35 Model acquired on a 73 km² wet grassland site and 2- more than 200 *relevés* collected in the
36 field.

37 **Results:** The results show that 1- the compromise typology yields significantly higher
38 mapping accuracy than classic phytosociological typology (62% and 26%, respectively); 2-
39 compared to a crisp approach, the fuzzy approach improves mapping accuracy by 17
40 percentage points and 3- a single plant community can be defined by several (1-4) distinct
41 spectral signatures.

42 **Conclusions:** The comprehensive fuzzy procedure successfully mapped herbaceous plant
43 communities at the ecosystem scale using inexpensive remote sensing data. Floristic and

44 spectral uncertainty was considered in a fuzzy approach, resulting in the mapping of 9
45 herbaceous plant communities with acceptable accuracy. As the natural habitats were
46 characterized at the plant community level, correspondence with functional properties of the
47 species or with ecosystem services can be easily inferred. These encouraging results open up
48 new ways to meet the requirements for monitoring the conservation status of natural habitats
49 in the EU Habitats Directive.

50 **Key-words:** LiDAR, noise clustering, phytosociology, Pléiades, remote sensing, vegetation
51 typology, wetlands.

52

53 **Nomenclature:** Gargominy et al. (2012) for vascular plants; Bioret et al. (2013) for plant
54 communities

55

56 **Running head:** Mapping plant communities using a fuzzy approach

57

58 **1 Introduction**

59 Faced with intensive agriculture, urbanization and climate change, the mapping and
60 monitoring of natural habitats is still a major challenge for conservation management. This
61 has very important consequences for herbaceous habitats (lawns, meadows) with strong
62 conservation stakes (Council Directive 92/43/EEC) that cover more than 30% of European
63 areas (Peeters 2009). Within this context, a spatio-temporal monitoring of natural habitats
64 over hundreds of km² is needed to meet reporting requirements for the conservation status of
65 European NATURA 2000 sites. To meet this requirement, natural habitats should be
66 identified at the plant community level in order to assess the heritage quality (Berg et al.
67 2014), ecosystem services (Lavorel et al. 2011) and impacts of agricultural practices or water
68 level management on vegetal biodiversity (Dumont et al. 2012; Stratford et al. 2015).

69 It seems as though remote sensing data are an attractive resource for monitoring the spatio-
70 temporal dynamics of natural grassland habitats (Vanden Borre et al. 2011). Numerous
71 studies have pointed out the contribution of satellite imagery for measuring species richness
72 (Rocchini et al. 2016) or predicting functional traits in grasslands (Lausch et al. 2016).
73 However, it remains a challenging task to accurately map grassland plant communities using
74 remote sensing data (Corbane et al. 2015; Lang et al. 2015), due to floristic uncertainty and
75 spectral uncertainty. The floristic uncertainty is the inevitable probability of misclassifying
76 vegetation *relevés* (De Cáceres et al. 2010), which is especially high when handling plant
77 communities with similar species compositions. Spectral uncertainty is related to the
78 misclassification of remote sensing data explained by the spectral similarities between plant
79 communities (Rocchini et al. 2013). The spectral response(s) of a plant community partially
80 reflect(s) its floristic composition (Rocchini & Cade 2008). Local contrasts in environmental
81 conditions, such as soil wetness and nutrient contents as well as individual plant interactions,
82 occur on very small scales, i.e. several square meters (Marion et al. 2010; Dumont et al.

83 2012). Consequently, the resulting fine-grained mosaic patterns of the vegetation show
84 variable spectral response(s) (Feilhauer et al. 2013; Kumar & Sinha 2014) and this spectral
85 variance reduces the distinctiveness of the various plant communities (Ali et al. 2016).
86 Conversely, grassland plant communities have a similar physiognomy, as they are dominated
87 by herbaceous graminoid species with a height range between 20 cm and 1 m in general. As a
88 result, the physiognomic similarity of grassland plant communities smooths out the spectral
89 variability between them (Rocchini et al. 2013).

90 To address these issues, many approaches have been developed to accurately map natural
91 habitats, such as (1) simplifying the vegetation typology at the expense of ecological
92 consistency, (2) using remote sensing satellite image time series, (3) considering vegetation as
93 a continuum rather than as plant communities and (4) applying fuzzy approaches:

- 94 1. Vegetation typologies have been created to fit spectral data variance, using
95 multivariate analyses such as canonical correlation analysis or redundancy
96 discriminant analysis. As a result, the spectral separability of the vegetation units is
97 improved and the vegetation units are accurately mapped (overall accuracy > 85%,
98 kappa index > 0.78) (Oldeland et al. 2010; Middleton et al. 2012). However, the
99 ecological consistency of the vegetation units mapped is altered. In fact, several plant
100 communities with a similar physiognomy or biomass are merged into the same
101 vegetation unit. At best, these vegetation units may be related to broad vegetation
102 classes (e.g. "Sparse grassland and open patches"; "Eutrophic fen") but in no way
103 correspond to meaningful plant communities *sensu stricto*, i.e. typology of the plant
104 associations (Bioret et al. 2013).
- 105 2. Several recent studies have investigated the contribution of multispectral satellite data
106 time series. For example, semi-natural grasslands were accurately mapped (overall
107 accuracy > 80%) using RapidEye (Schmidt et al. 2014) or Sentinel-2A (Shoko &

108 Mutanga 2017) multispectral time series. However, only the dominant vegetation
109 patches were distinguished due to the relatively coarse spatial resolution of these time
110 series (6-10 m), which is insufficient to identify patches of small, long or thin plant
111 communities (Roth et al. 2015). Another study highlighted the contribution of
112 TerraSAR-X time series to accurate mapping of 7 grassland habitats (overall accuracy
113 90%, kappa index 0.89) with a 2 m spatial resolution (Schuster et al. 2015). However,
114 these SAR time series remain expensive.

115 3. Other studies have focused on mapping the floristic *continuum* rather than mapping
116 plant communities. For example, the floristic *continuum* was mapped with high
117 accuracy ($r^2 > 0.8$) using airborne hyperspectral imagery of raised-bog (Schmidtlein et
118 al. 2007) or heath habitats (Neumann et al. 2015). In addition, Feilhauer et al. (2014)
119 successfully mapped local variability in complex mire habitats using Rapideye and
120 Sentinel-2 simulated multispectral imagery ($r^2 > 0.7$, overall accuracy 0.71) .
121 However, these promising approaches are not yet operational for wide use to report
122 the requirements of Habitat Directive in natural habitats as they have been developed
123 for specific environments, such as raised bogs, mires or heaths covering a few
124 hectares; lower accuracy was observed when mapping dry heaths and pioneer
125 grassland habitats (Neumann et al. 2015).

126 4. A well-known approach for dealing with uncertainty is the fuzzy approach (Zadeh
127 1965). Unlike the widely applied crisp approaches, the fuzzy approach assigns a
128 probability of membership in each class to each individual. This property is useful for
129 addressing floristic and spectral uncertainty and assessing the confidence level of the
130 classification of a given plant community to one or more spectral response(s). Until
131 now, the fuzzy approach has been applied widely to classify vegetation *relevés* (De
132 Cáceres et al. 2010; Wiser & Cáceres 2013; Duff et al. 2014) or remote sensing data.

133 For example, Zlinszky et al. (2014; 2015) mapped herbaceous habitats with 68% and
134 62% overall accuracy, respectively (kappa index 0.64 and 0.58, respectively), using
135 point-cloud LiDAR data. But the combined use of fuzzy classification based on both
136 vegetation and remote sensing data still remains to be investigated (Rocchini 2014).

137 The objective of this study was to accurately map grassland plant communities using a
138 comprehensive fuzzy approach in order to address the floristic and spectral uncertainty. To do
139 this, we first created a vegetation typology that is both ecologically and spectrally consistent
140 in terms of performing a dimensional scaling of the floristic and spectral values derived from
141 vegetation *relevés* and remote sensing data, respectively. Second, we mapped grassland plant
142 communities using the noise clustering classifier. The strengths and weaknesses of the
143 methodology proposed will be discussed below.

144
145

146 **2 Material and methods**

147 *2.1 Study area*

148 The study site, a large area spanning 73 km² in a Natura 2000 site, is the second largest
149 French wetland area, located in the Poitevin marsh, close to the French Atlantic coast
150 (46.4°N, 1.2°W) (**Fig. 1**). The climate is oceanic temperate, with a mean monthly
151 minimum/maximum temperature ranging from 2/10°C in winter to 12/24°C in summer. The
152 annual mean precipitation ranges from 700 to 900 mm with a summer water deficit. Coming
153 from a successive embankment since the 10th century, this marsh has a relatively flat
154 geomorphology with slight depressions. The elevation ranges between 1.5 and 3.5 m above
155 sea level. The grasslands are extensively grazed or mown. They are composed of sub-brackish
156 herbaceous plant communities, driven by a flooding pattern (Amiaud et al. 1998) and grazing
157 pattern (Marion et al. 2010), that correspond to Natura 2000 class 1410.3 (thermo-Atlantic

158 and sub-brackish meadows), EUNIS class A2.523 (Mediterranean short *Juncus*, *Carex*,
159 *Hordeum* and *Trifolium saltmeadows*) and CORINE class 15.52 (Mediterranean short rush,
160 sedge, barley and clover saltmarshes).

161

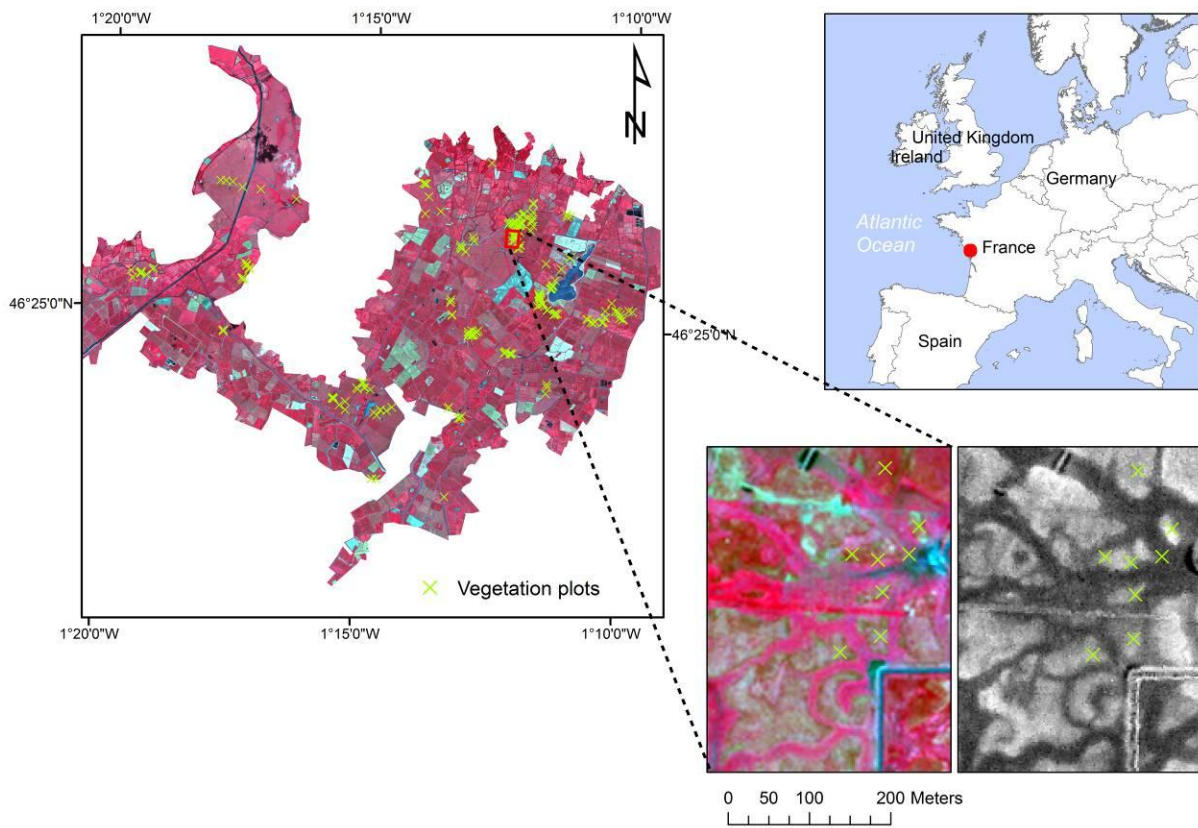


Fig. 1. Study site and vegetation plot location. False-colour composite of a Pléiades image (© CNES ISIS) located in the Poitevin marsh (France). The inserts show a subset of the grassland pattern on the Pléiades image (left) and the LiDAR-derived Digital Terrain Model (right).

162

163 The overall methodology developed in this study is detailed in **Figure 2**.

FUZZY CLASSIFICATION OF VEGETATION RELEVÉS

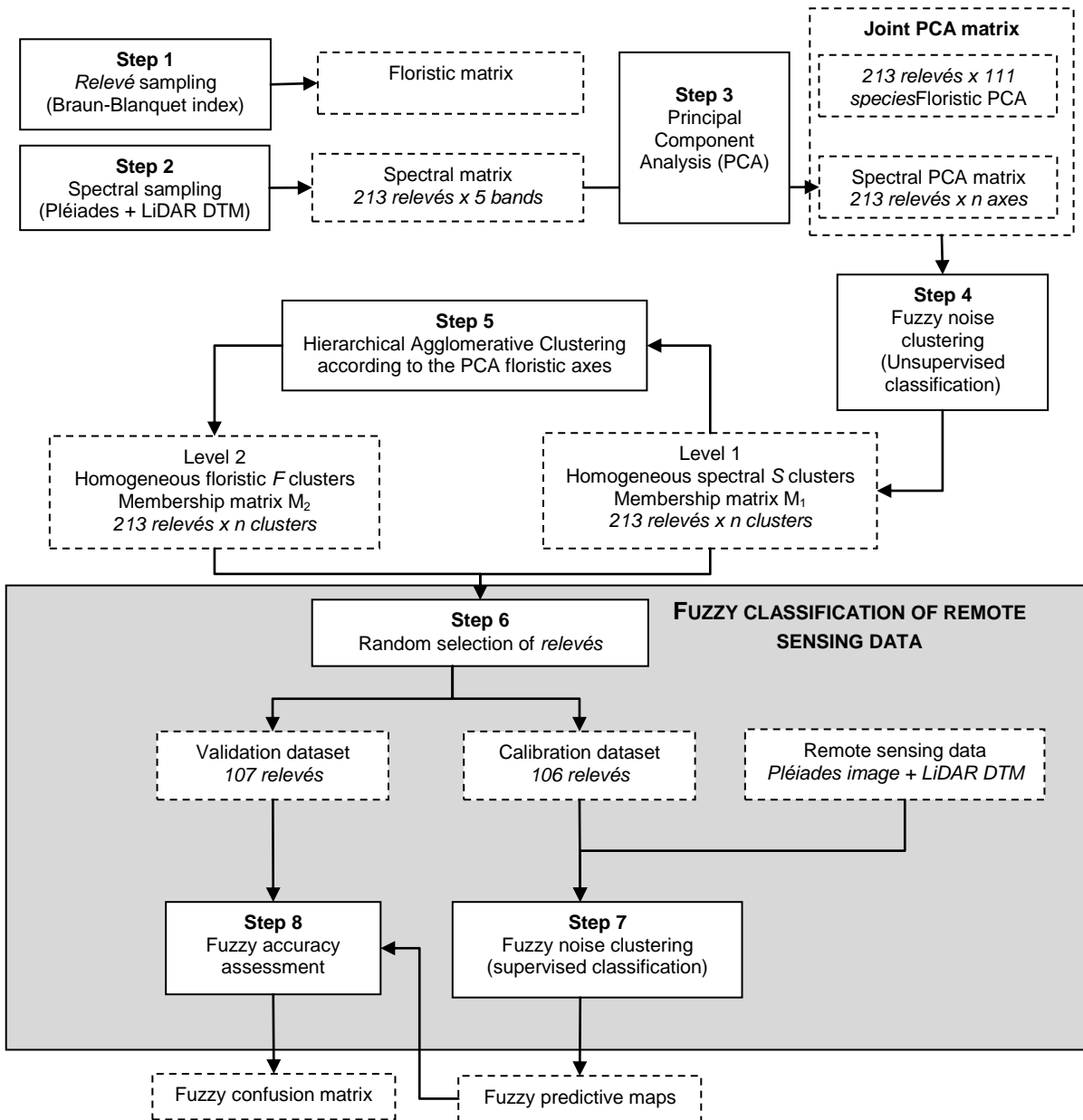


Fig. 2. Methodological flowchart detailing the comprehensive fuzzy approach. First (top), *relevés* were classified using a fuzzy noise clustering classifier; then (bottom), this fuzzy model was predicted from remote sensing data.

166 2.2.1 Step 1. Vegetation relevé sampling

167 Due to the spatial resolution of the Pléiades imagery (2 m), we selected vegetation *relevés*
168 within a 6 m × 6 m quadrat to avoid mixed pixels. Vegetation *relevés* were collected in the
169 field from May to June 2015. To stratify the field sampling, unsupervised classification (20
170 classes) was performed on a Pléiades satellite image acquired in May 2013. This 20-class map
171 was loaded in the field computer and helped us to identify main spatial patterns within
172 grasslands. Following the traditional phytosociological rule (Dengler 2017), *relevés* were
173 collected within plots with *a priori* homogeneous floristic composition. For each vegetation
174 *relevé*, the number of vascular plant species was recorded ($n = 111$ for all plots) and their
175 abundance was estimated using the Braun-Blanquet approach (Braun-Blanquet 1932). In total,
176 220 vegetation *relevés* were geo-referenced using a differential GPS (error < 0.5 m) and
177 recorded in the vegetation database TURBOVEG (Hennekens & Schaminée 2001).

178 2.2.2 Step 2. Spectral sampling

179 This step associates vegetation *relevés* with reflectance spectra extracted from remote sensing
180 data. A multispectral Pléiades image was used in combination with LiDAR (Light Detection
181 and Ranging) data. We used a multispectral Pléiades image because it presents a good trade-
182 off between cost (€1/km²), spatial resolution and coverage (15 km x 15 km). The Pléiades
183 image (© CNES ISIS program) was acquired in June 2014 and features a high spatial
184 resolution (2 m) with 12-bit depth spectral information in the blue (443-550 nm), green (490-
185 610 nm), red (590-710 nm) and near infrared (740-940 nm) regions. The Pléiades image was
186 delivered at Level-1B, which includes inter-detector normalization, inter-array reconstruction
187 and geometric corrections (Panem et al. 2012). The image was orthorectified using a LiDAR
188 Digital Terrain Model (DTM). The horizontal error of the rectified image was less than 1
189 pixel. The Pléiades image was atmospherically corrected using the MODTRAN-4 model
190 (Adler-Golden et al. 1999). In addition, we integrated a LiDAR DTM in the vegetation

191 modelling as vegetation strongly responds to elevation contrasts (Moeslund et al. 2011;
192 Rapinel et al. 2015; Alexander et al. 2016). Airborne LiDAR data were acquired in November
193 2011 by the French Mapping Agency (IGN - Institut Géographique National). Only the
194 LiDAR-derived DTM was subsequently delivered (grid size 1 m, vertical accuracy 0.2 m); the
195 raw point cloud was unavailable. Although some topographical variables such as the
196 Topographic Wetness Index (TWI) and Topographic Position Index (TPI) have been relevant
197 for mapping plant communities in wetlands (Alexander et al. 2016), we did not use them
198 because 1- the TWI is not suited for wetlands such as the Marais Poitevin, in which
199 anthropogenic features such as pipes and ditches have altered natural hydrological runoff
200 (Lindsay & Dhun 2015); and 2- the TPI – which expresses elevation relative to that of the
201 stream is scale-dependent (Alexander et al. 2016). To address these concerns, we chose to
202 express elevation as the depression elevation (Alber & Piégay 2011). This DTM was modified
203 to be expressed relative to the depression elevation instead of the sea level by subtracting the
204 absolute value of the DTM from the altimetric reference plan corresponding to the local
205 depression slope (see Alber & Piégay (2011) for a detailed description of the methodology).
206 The reflectance spectra associated with the vegetation *relevés* were taken from the Pléiades
207 image and the modified DTM. Then, the values of the pixels included within each vegetation
208 *relevé* were averaged. To avoid ambiguities between ground data and remote sensing
209 imagery, we verified the homogeneity of the Pléiades spectral responses when calculating the
210 Euclidean distance between the spectra within each vegetation *relevé*. Seven heterogeneous
211 vegetation *relevés* were removed, leaving 213 plots for the analysis.

212 2.3 Creation of a typology using the vegetation *relevés*

213 2.3.1 Step 3. Independent PCA applied to the floristic matrix and spectral matrix

214 This step builds a “joint” matrix that includes both spectral and floristic dimensionally-
215 reduced data. Many studies have shown the interest of unconstrained ordination such as a

216 principal component analysis (PCA) to summarize the floristic variance (Legendre &
217 Gallagher 2001). The main advantage of the PCA method compared to the non-metric
218 multidimensional scaling (NMDS) method is that a difference between the abundance values
219 for a common species contributes more to the distance than the same difference for a rare
220 species, so that rare species may have a limited influence on the analysis. Therefore, the PCA
221 method is better suited to our dataset because plant communities are more likely to differ by a
222 variation in the abundances of the dominant species rather than the occurrence of rare species.
223 As a preprocess, the Braun-Blanquet cover values on floristic data were replaced with the
224 median cover values of each class (1 = 0.03; 2 = 0.13; 3 = 0.375; 4 = 0.625; 5 = 0.875) in
225 order to linearize the cover values. Then, the cover values were submitted to a Chord
226 transformation (i.e. divided by the norm). These transformations must be done before
227 performing a PCA on this type of floristic dataset to ensure that the Euclidean distances
228 between the vegetation *relevés* calculated from the plant cover values accurately reflect the
229 floristic similarities between the *relevés* (Legendre & Gallagher 2001). We performed two
230 distinct PCAs: a first PCA on the floristic data and a second PCA on the spectral data. As the
231 floristic and spectral matrices have completely different value ranges, each dataset was scaled
232 separately using centered scaling before PCA. Last, we built a “joint” PCA matrix with the n
233 axes scores of the floristic PCA and the n axes scores of the spectral PCA.

234 2.3.2 Step 4. Fuzzy noise clustering (unsupervised classification)

235 This step classifies vegetation *relevés* into spectrally separable clusters with a fuzzy approach.
236 In vegetation science, a fuzzy classification recognizes that certain vegetation *relevés* may
237 correspond to a transition between many plant communities and as a result, they could have
238 an uncertain classification. The joint PCA matrix was used as basis for the unsupervised fuzzy
239 classification of the vegetation *relevés*. As the joint PCA matrix contains data from both
240 floristic and spectral PCA, the unsupervised classification should cluster *relevés* that share

241 both floristic and spectral similarities. We used a noise clustering classifier (NC) (De Cáceres
242 et al. 2010), a prototype-based clustering method derived from the C-means (Bezdek et al.
243 1984), to find c clusters and assign n plots to these c clusters so that the resulting clusters are
244 compact and distinct from each another. The NC classifier results in a fuzzy classification
245 because a cluster membership probability is assigned to each vegetation *relevé* where the sum
246 of the membership probabilities is equal to 1. The NC classifier also identifies "noise" *relevés*
247 resulting from rare spectral or floristic values. The advantage is that "noise" *relevés* do not
248 affect the cluster centers. Hence, the centers of interest are ultimately more distinct from each
249 other (De Cáceres 2016). The main input parameters for the NC algorithm are the number of
250 clusters created by the method (mC), the fuzziness coefficient (m) and the distance to the
251 noise cluster (δ). A high m value will lead to a classification where the probabilities of
252 belonging to a cluster are more distributed over several clusters while a low δ value will
253 increase the number of plots attributed to the noise cluster. Based on preliminary tests
254 performed on our dataset, we set the intervals of input parameters as follows: mC 15-30 using
255 a step of 1, m 1.1-1.9 using a step of 0.1 and δ 1.5-2.0 using a step of 0.1. After completing
256 the fuzzy classification process, we called M_I the resulting membership matrix that gives, for
257 each vegetation *relevé*, the respective probabilities of belonging to the different spectrally
258 homogeneous S clusters, i.e. one with low spectral variance.

259 2.3.3 Step 5. Hierarchical agglomerative clustering

260 This step groups the spectrally homogeneous clusters into floristically homogeneous clusters.
261 Level 1 corresponds to the spectrally homogeneous S clusters (i.e. with low spectral
262 variability within clusters). They were derived from the NC classifier of the joint PCA matrix
263 but with classifier parameters that minimized spectral variability to the detriment of floristic
264 variability. The higher Level 2 corresponds to the floristically homogeneous F clusters (i.e.
265 with low floristic variability within clusters) that were derived from the initial Level 1 clusters

266 merged with hierarchical agglomerative clustering based on floristic PCA axes. Here, we
267 hypothesized that a given plant community (Level 2) may have several distinct spectral
268 signatures (Level 1). For this reason, it is important to first identify spectrally homogeneous
269 clusters discernible on remote sensing data. The main input parameter for HAC is the
270 threshold value, which determines the final number of clusters. As a result, a second
271 membership matrix M_2 containing the probabilities of belonging to the F clusters (Level 2)
272 was created by summing the membership probabilities of the agglomerated S clusters (Level
273 1) from M_1 . Expert-based assignment was then applied between the floristically homogeneous
274 F clusters (Level 2) and the French phytosociological system (Bioret et al. 2013).

275 2.3.4 Search for optimal clustering parameters

276 In order to find the best clustering parameter values (mC , m , δ , *HAC threshold*), we carried
277 out a major tuning procedure that repeated steps 3-5 with different combinations of the
278 parameter values. Our objective was to find an optimal trade-off classification for the
279 vegetation *relevés* that respects three criteria: 1- having homogeneous spectral clusters at M_1 ,
280 2- having homogeneous floristic clusters at M_2 and 3- having at least 60% of the vegetation
281 *relevés* classified with a maximum membership higher than 0.4. The homogeneous spectral
282 clustering was assessed based on two geometric indices - the average silhouette value
283 (Rousseeuw 1987), which geometrically evaluates the quality of the clustering, and Hubert's
284 C-index (Hubert & Arabie 1985), which compares the partition obtained with the best
285 partition that could have been obtained with this number of groups and this distance matrix.

286 The homogeneous floristic clustering was assessed based on an ecological index, the fidelity
287 coefficient phi (Chytrý et al. 2002) (only species with $\text{phi} \geq 0.2$ were considered as diagnostic
288 species), in combination with average silhouette value and Hubert's C-index. The average
289 silhouette value and Hubert's C-index assess whether the clusters are compact and distinct

290 from each other while the phi coefficient specifically assesses whether a cluster contains
291 diagnostic species, which are crucial for identifying vegetation units (De Cáceres et al. 2015).

292 The optimal clustering parameters were determined to correspond to the maximum (for the
293 average silhouette value and number of diagnostic species) and minimum values (for Hubert's
294 C-index) of three selected indices and should result in the best trade-off classification of the
295 vegetation *relevés* with regards to their homogeneous spectral and floristic clusters.

296 *2.4 Fuzzy classification of remotely sensed data*

297 *2.4.1 Step 6. Random selection of the relevés*

298 This step randomly assigns each *relevé* to the calibration or validation dataset. In the
299 supervised classification of RS data, all *relevés*, including noise *relevés*, were used. The
300 classified vegetation *relevés* were equally and randomly split into two datasets: 1- the
301 calibration dataset used for the supervised NC classifier and 2- the validation dataset used to
302 assess the accuracy of the classified remote sensing data. Both calibration and validation
303 datasets included the M_1 and M_2 matrices.

304 *2.4.2 Step 7. Fuzzy noise clustering (supervised classification)*

305 This step applies the noise clustering model to all pixels of the remote sensing image. Usually,
306 the field samples used to classify remote sensing data have a crisp assignment to a single
307 cluster. Here, we assume that a vegetation *relevé* has a probability of belonging to each
308 cluster. For this reason, the remote sensing data were classified using the NC, which preserves
309 the fuzzy assignment of the vegetation *relevés* (see step 4). A supervised classification of
310 remotely sensed data was performed using the homogeneous spectral matrix M_1 in the
311 calibration dataset. The classification produced a membership matrix CM_1 giving, for each
312 pixel, its probabilities of belonging to each homogeneous spectral cluster. Then, the
313 memberships of CM_1 were summed based on the aggregation rules defined in the HAC

314 analysis (step 5). This resulted in a CM_2 matrix giving, for each pixel, its probabilities of
315 belonging to each homogeneous floristic cluster. At the end of the classification procedure, a
316 set of fuzzy maps was produced for each vegetation cluster. To obtain a crisp map of the
317 vegetation cluster based on crisp classification, the membership matrix CM_2 was defuzzified
318 by attributing, to each pixel, the class for which it had the highest membership probability. In
319 addition, two other classes were considered: 1- the noise class, generated by the NC classifier
320 and composed of the outliers, and 2 – the unclassified class, corresponding to pixels with a
321 maximum CM_2 membership probability less than 0.4 (below which there is no clear majority
322 among clusters).

323 2.4.3 Step 8. Fuzzy accuracy assessment

324 This step measures the accuracy of the fuzzy classification of the remote sensing image. The
325 traditional crisp calculation of the confusion matrix requires the defuzzification of the fuzzy
326 map. To avoid losing membership information, we chose to calculate a fuzzy confusion
327 matrix from the fuzzy predicted and reference membership matrices following Binaghi et al.
328 (1999). Finally, a fuzzy kappa was calculated using Cohen's kappa coefficient to measure the
329 agreement between the fuzzy sets proposed by (Dou et al. 2007). Details of the calculations
330 are given in Appendix S1. *Relevés* with a maximum membership probability less than 0.4
331 among the 9 vegetation clusters were considered "unclassified". However, their membership
332 probabilities were included when calculating the confusion matrix. To compare accuracy
333 results to those of a traditional crisp classifier, *relevés*' membership probability for the noise
334 class was not considered when assessing the accuracy.

335 To avoid any bias due to the selection of the calibration and validation data, the remotely
336 sensed data classification procedure (from step 6 to step 8) was repeated 1000 times with
337 randomly selected calibration and validation datasets. The classification with the median
338 overall accuracy value was selected as the final fuzzy classification output.

339

340 2.5 Assessment of the fuzzy noise clustering approach

341 In order to assess the relevance of our approach to existing ones, we compared the overall
342 accuracy of the vegetation maps derived from: (i) a fuzzy and a crisp classification, (ii) our
343 “trade-off” typology with a floristic typology on the one hand and a physiognomic typology
344 on the other hand. Crisp classification of the remote sensing data was performed using the
345 crisp vegetation dataset (by defuzzifying the M_2 membership matrix, i.e. assigning each *relevé*
346 to a vegetation cluster based on its highest membership probability) with a support vector
347 machine (SVM) algorithm that is widely recognized as the most efficient classifier
348 (Mountrakis et al. 2011). The optimal calibration model was defined by a 10-fold cross-
349 validation sampling method. The floristic typology was constructed based on the scores of the
350 floristic PCA axes. Conversely, the physiognomic typology was based on the score of the
351 spectral PCA axes.

352 All analyses were performed in the R 3.1.2 statistical environment (R Core Team 2015) using
353 the packages *vegan* (v 2.3-4) (Oksanen et al. 2015), *vegclust* (v 1.6.3) (De Caceres 2016),
354 *ade4* (v 1.7-4) (Dray & Dufour 2007), *raster* (v 2.5-2) (Hijmans 2015) and *rgdal* (v 1.1-3)
355 (Bivand et al. 2015).

356

357 3 Results

358 3.1 Classification of the vegetation relevés

359 The numbers of dimensions considered in the floristic and spectral PCA, respectively, were
360 set to three for each PCA. As a result, the NC classification was performed on PCA matrix M_1
361 which contained six variables explaining 38.1% and 97.8% of the floristic and spectral
362 variance, respectively. The fuzziness coefficient ($m = 1.7$) as well as the distance to the noise

363 cluster ($\delta = 1.7$) values were quite large with the result that 35.2% and 2.3% of the total plots
364 fell into the unclassified (i.e. maximum class membership < 0.4) and noise clusters,
365 respectively. The number of initial clusters was set to $mC = 15$ for M_1 and merged to form
366 nine final clusters (M_2) after the agglomerative hierarchical clustering ($dt = 0.6$).

367 Figure 3 clearly illustrates the weak relationship between the spectral and floristic variance
368 and the interest of the nested-level approach: at level 1, the S clusters had similar spectral
369 values (average silhouette value = 0.15) but quite different floristic values with a high intra-
370 class variance (average silhouette value = 0.10). Conversely at level 2, the F clusters had
371 similar floristic values (average silhouette value = 0.21; Hubert's C index = 0.12) and were
372 characterized by at least one diagnostic species ($n = 56$) but had quite different spectral values
373 (average silhouette value = -0.02). As an example, at level 1, clusters S6 and S11 had similar
374 floristic values that overlap (**Fig. 3**, upper right) but which could be clearly distinguished by
375 their clear spectral differences (**Fig. 3**, upper left). At level 2, these two clusters were merged
376 together into a F6 cluster with similar floristic values (**Fig. 3**, bottom right) but with spectral
377 values spread out between clusters F2 and F5. Dendrogram and silhouette plots are presented
378 Appendix S2.

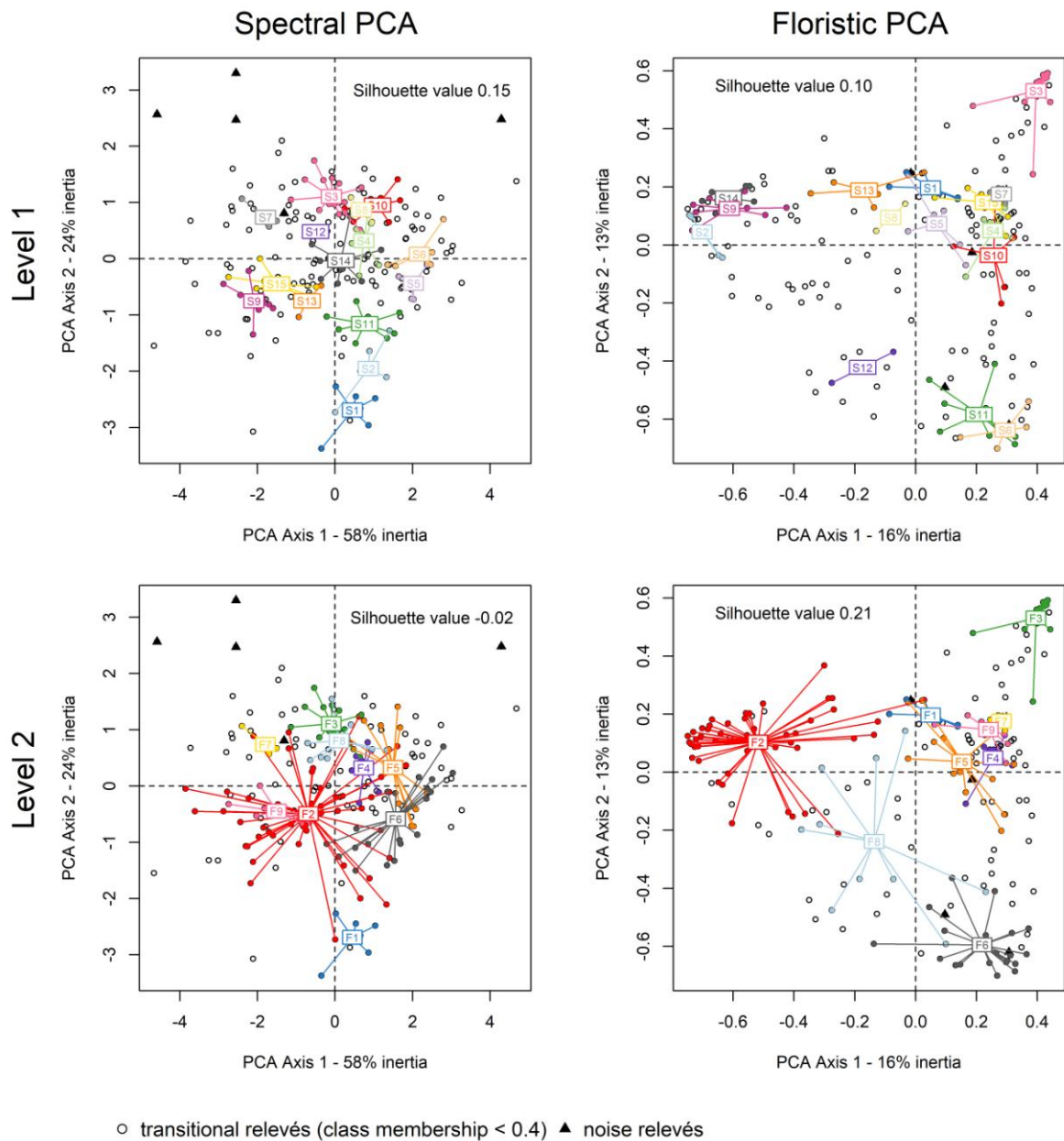


Fig. 3. Weak relationship between spectral and floristic variance and the utility of the nested-level approach. For visualization purposes, scaled principal component analyses (PCA) were performed at level 1 (top) and level 2 (bottom) on the spectral (left) and floristic (right) values. Each cluster derived from noise clustering of the joint PCA matrix is represented by a code and a colour.

379

380 The floristic composition of each final cluster together with the number of initial clusters are
 381 shown in **Table 1**. Correspondence with the French national nomenclature is also provided
 382 based on expert interpretation and diagnostic species (Table 2). In further detail, clusters F1 to
 383 F2 are typical of hygrophilous (annual flood duration > 4 months) and grazed grasslands:

384 cluster F1 is related to the *Urtico dioicae-Phalaridetum arundinaceae* plant community while
385 cluster F2 corresponds to the *Eleocharito palustris-Oenanthetum fistulosae* plant community
386 variation at *Ranunculus ophioglossifolius*. Cluster F3 is related to meso-hygrophilious (annual
387 flood duration between 1 and 3 months) and grazed grasslands corresponding to the
388 *Alopecuro bulbosi-Juncetum gerardii* plant community. Cluster F4 is related to meso-
389 hygrophilious grasslands with alternative grazing and mowing corresponding to the *Trifolio*
390 *maritimi-Oenanthetum silaifoliae* plant community. Clusters F5 and F6 are related to meso-
391 hygrophilious and mown grasslands corresponding respectively to the *Junco gerardi-*
392 *Oenanthetum fistulosae* and *Elytrigio repentis-Caricetum divisae* plant communities. Clusters
393 F7 and F8 are very similar and correspond to mesophilious (annual flood duration < 1 month)
394 and grazed grasslands related to the *Carici divisae-Lolietum perennis* plant community.
395 Cluster F8 is found on more intensively grazed grasslands. Cluster F9 is found in mesophilous
396 grasslands with alternative grazing and mowing phases and corresponds to the *Hordeo*
397 *secalini-Lolietum perennis* plant community.

398 Notably, four clusters (F2, F5, F6 and F8) are characterized by two or more spectral
399 signatures (S clusters, level 1) while five other clusters (F1, F3, F4, F7 and F9) are
400 characterized by one spectral signature (Table 1).

401 **Table 1.** Synoptic table of the vegetation units in the Poitevin marsh. Frequency values (in percentages) of the
 402 species in the clusters obtained from the noise clustering classifier. Diagnostic species are indicated in gray (phi
 403 ≥ 0.20) and dark gray (phi ≥ 0.40). The full version is available in Appendix S3.

DOMINANT AGRICULTURAL PRACTICES	Grazing		Mowing				Grazing		
	4 months		1-3 months				< 1 month		
CLUSTER NAME (LEVEL 2)	F1	F2	F3	F4	F5	F6	F7	F8	F9
NUMBER OF INITIAL CLUSTERS (LEVEL 1)	1	4	1	1	2	2	1	2	1
<i>Eleocharis uniglumis</i>	43	8							
<i>Phalaris arundinacea</i>	29	3				5			
<i>Agrostis stolonifera</i>	57	97	7	29	46	50	20	100	38
<i>Glyceria fluitans</i>	43	46			8				
<i>Oenanthe fistulosa</i>	29	74			8	55			38
<i>Ranunculus repens</i>	14	59			15	10	20		
<i>Eleocharis palustris</i>	57	49			15	5			
<i>Mentha pulegium</i>	14	41			15	5			
<i>Trifolium fragiferum</i>	14	46	7		15				38
<i>Hordeum marinum</i>		3	87		8		20		
<i>Juncus gerardi</i>		8	100		23	25	40	20	13
<i>Parapholis strigose</i>			47						
<i>Plantago coronopus</i>			87		23		60	10	
<i>Holcus lanatus</i>		5		100	31	25		10	25
<i>Festuca arundinacea</i>		3		29		10			
<i>Tragopogon porrifolius</i>				29					
<i>Medicago littoralis</i>				29					
<i>Trifolium pratense</i>				43					13
<i>Trifolium maritimum</i>			20	86	54	25	100	20	
<i>Anthoxanthum odoratum</i>		3		71	54	20		30	13
<i>Elytrigia repens</i>		21	20	29	77	100	20	90	38
<i>Carex divisa</i>		15	53	71	62	95	40	100	13
<i>Leontodon hispidus</i>							60		
<i>Trifolium subterraneum</i>							40		25
<i>Hypochaeris radicata</i>				14			40	10	13
<i>Iris spuria</i>								40	
<i>Bromus racemosus</i>			27	29	8		40	70	25
<i>Cynosurus cristatus</i>				43	31	10	80	80	38
<i>Cirsium species</i>								20	
<i>Hordeum secalinum</i>	14	23	20	43	46	10	20	80	63
<i>Lolium perenne</i>		5	20	43	38	5	100	70	100
<i>Trifolium repens</i>				14	8			10	38
<i>Ranunculus acris</i>		3							50

404

405

406

407 3.2 Classification of remotely sensed data

408 The supervised fuzzy noise clustering classification of remotely sensed data produced three
409 sets of maps: class membership maps for each plant community (**Fig. 4**, left), an uncertainty
410 map (**Fig. 4**, right) and a crisp classification map (Appendix S5). To improve visualization of
411 the fuzzy classification, class membership maps for each plant community were featured
412 using hue-preserving colour blending (Chuang et al. 2009). The main advantages are that each
413 vegetation cluster has a specific colour and that the colour's saturation level indicates the
414 certainty of class assignment (Zlinszky & Kania 2016). The spatial distribution of grassland
415 habitats along wetlands is consistent with their ecological *preferendum*: for example, cluster
416 F2 is clearly distributed in topographical depressions and long-term flood areas while clusters
417 F7 and F8 occur at higher elevations that are rarely flooded. Notably, cluster F3 is linearly
418 distributed along topographical slopes. Interestingly, the map of the noise cluster highlights
419 non-grassland habitats such as channels, crops and bare soils but also noisy pixels such as tree
420 shadows and flooded vegetation. The uncertainty map reveals transitional areas between two
421 plant communities.

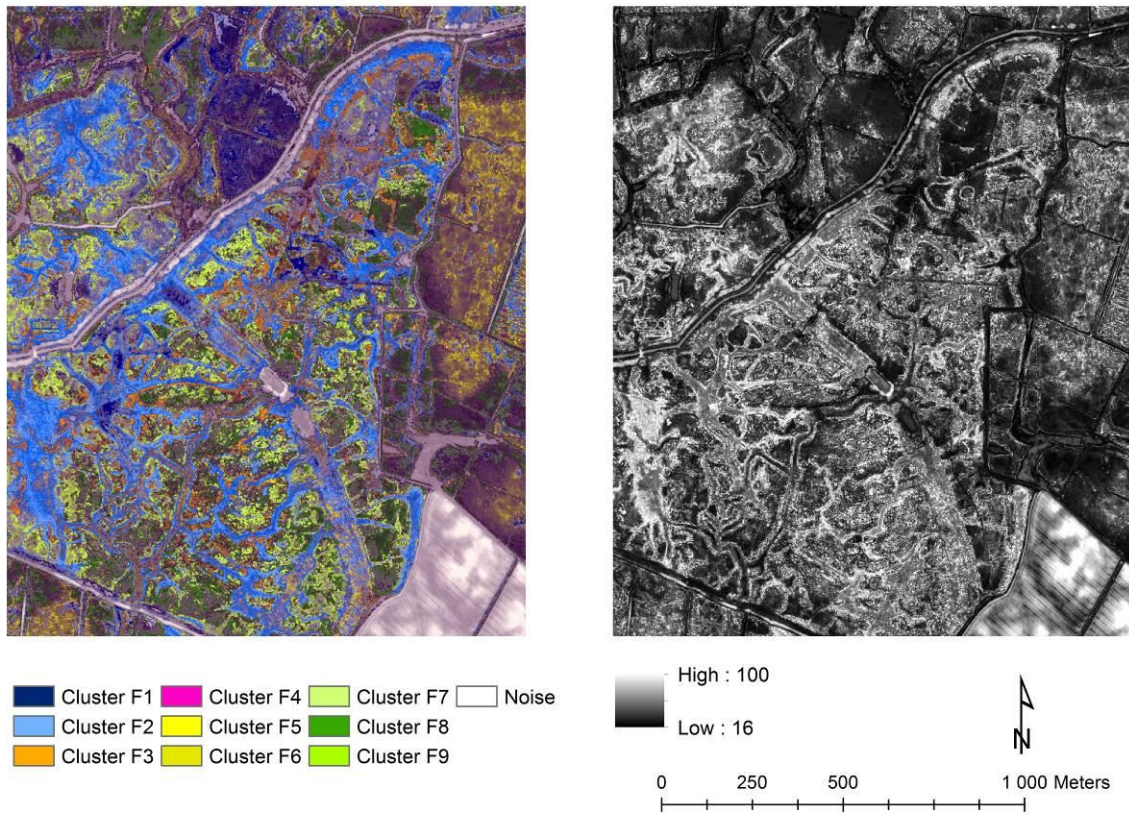


Fig. 4. Subset of classified vegetation maps derived from the fuzzy noise clustering: the fuzzy blended image (left) using the hue-preserving algorithm (see Zlinszky and Kania (2016)) shows gradual transitions between classes; the uncertainty image (right) shows areas of high uncertainty in black and more certain areas in white.

422

423 The iterative process of random selection of calibration and validation dataset shows low
 424 variation in overall accuracy (standard deviation = 1.7). The median fuzzy confusion matrix
 425 shows an overall accuracy of 62% (Table 2). The producer's accuracy values are higher than
 426 60% for all clusters except for clusters F3, F4 and F9. The user's accuracy values are higher
 427 than 60% for all clusters, except for clusters F1, F6 and F9. The reference and classified
 428 membership matrices are available in Appendix S4. The importance of spectral bands to
 429 classification accuracy is detailed in Appendix S6.

430 Table 2. Fuzzy accuracy assessment of the map of plant communities derived from remote sensing imagery:
 431 overall accuracy (%), Kappa index, producer's accuracy (%) and user's accuracy (%) for each cluster.

Cluster	Plant community	Producer's Accuracy	User's Accuracy
F1	<i>Urtico dioicae - Phalaridetum arundinaceae</i>	60	57
F2	<i>Eleocharito palustris-Oenanthetum fistulosae</i> variation at <i>Ranunculus ophioglossifolius</i>	69	60
F3	<i>Alopecuro bulbosi-Juncetum gerardii</i>	56	60
F4	<i>Trifolio maritimi-Oenanthetum silaifoliae</i>	43	65
F5	<i>Junco gerardi - Oenanthetum fistulosae</i>	67	61
F6	<i>Elytrigio repentis-Caricetum divisae</i>	63	42
F7	<i>Carici divisae-Lolietum perennis</i> variation at <i>Plantago coronopus</i> and <i>Bellis perennis</i>	65	63
F8	<i>Carici divisae-Lolietum perennis</i>	68	68
F9	<i>Hordeo secalini-Lolietum perennis</i>	40	25
Median overall accuracy 62 %			
Median Kappa index 0.56			

432

433 3.3 Impact of the typology and fuzzy approach on map accuracy

434 The influence of our trade-off typology and fuzzy approach on map accuracy is presented in
 435 **Fig. 5**. It highlights a clear trade-off between the overall accuracy of the classification and the
 436 floristic significance of the typology. When the floristic typology is applied (Fig. 5, left), the
 437 clusters have consistent floristic values (average silhouette value = 0.26) but the overall
 438 accuracy of the classification remains very low, either with a fuzzy (25.9%) or a crisp (26.1%)
 439 classification approach. Conversely, when a spectral typology is applied (Fig. 5, right), the
 440 overall accuracy of the classification is excellent either with a fuzzy (92.8%) or crisp (90.6%)
 441 classification approach but the clusters have quite different floristic values (average silhouette
 442 value = -0.03). Using the compromise typology (Fig. 5, middle), the clusters are not only
 443 comprised of similar floristic values (average silhouette value = 0.21) but they also contain
 444 distinct spectral values (overall accuracy = 62%) when a fuzzy classification is performed. In

445 the case of the compromise typology, the fuzzy classification (overall accuracy = 62%)
446 significantly outperforms the crisp classification (overall accuracy = 44.8%).

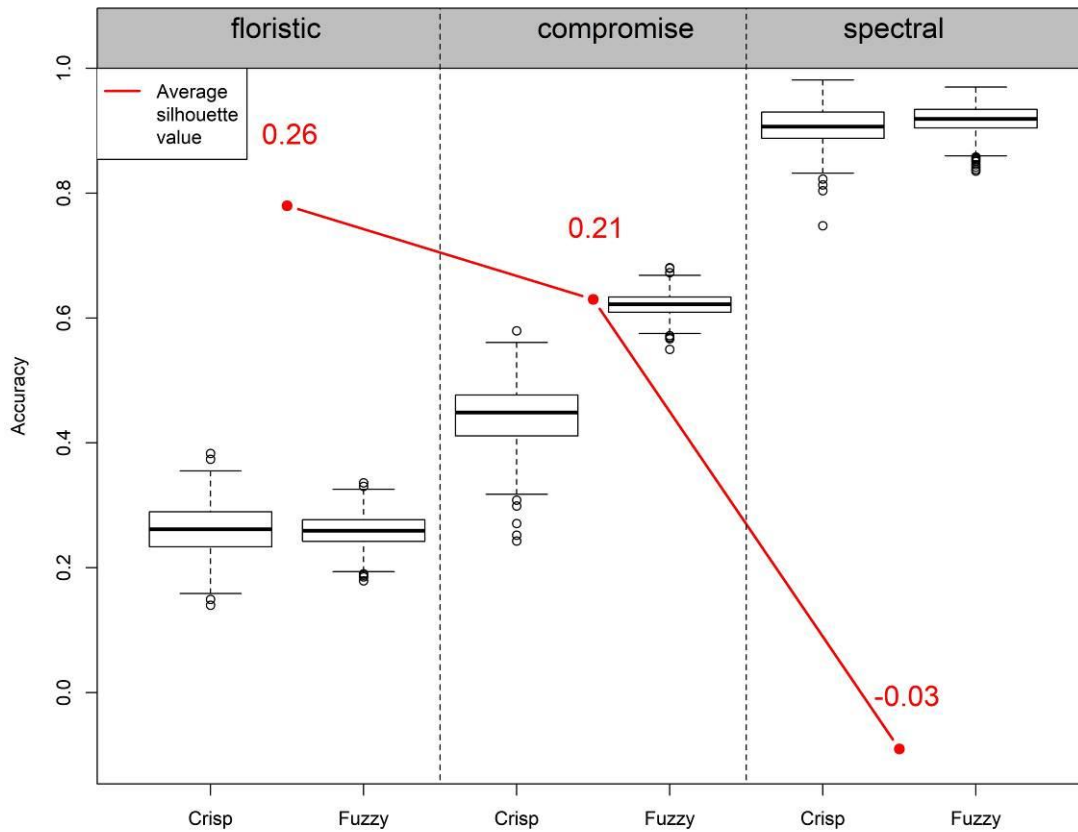


Fig. 5. Trade-off between mapping accuracy (expressed as the overall accuracy percentage) and floristic coherence of the typology (expressed as the average silhouette value). Boxplots were calculated from 1000 iterations of random selection of calibration and validation *relevés*.

447

448 **4 Discussion**

449 The aim of this study was to map grassland plant communities on a large wetland site (73
450 km²) combining a cost-effective satellite multispectral image and a LiDAR-derived DTM. We
451 developed a novel approach that combines a compromise typology and a fuzzy approach. The
452 grassland plant communities were classified and mapped with 62% accuracy (kappa index
453 0.56), which is acceptable considering the area of the study site, the detailed typology (9

454 clusters, each representing a grassland with a similar physiognomy) and the inexpensive
455 remote sensing data used. In comparison, Kumar and Sinha (2014) achieved an accuracy of
456 42% using satellite multispectral imagery on a 9.5 km² salt marsh; Roelofsen et al. (2014)
457 achieved an accuracy of 59% (kappa index 0.46) using airborne hyperspectral imagery alone
458 on a 12 km² coastal marsh and Zlinszky et al. (2014; 2015) mapped herbaceous habitats with
459 68% and 62% overall accuracy, respectively (kappa index 0.64 and 0.58, respectively), using
460 point-cloud LiDAR data of meadows covering a few hectares. The maps we produced appear
461 to reliably detect and report on plant communities. It provides a valuable source of data to
462 assess and monitor the conservation status of natural habitats. Together with trait-based maps
463 (Lausch et al. 2016), this type of floristically-sensitive vegetation map will open up new
464 avenues for documenting habitat-related ecosystem services.

465 *4.1 Significance of method used to develop the typology*

466 We aimed to develop a vegetation typology that is both ecologically and spectrally consistent
467 (**Fig. 5**). Given the weak relationship between spectral variance – derived from inexpensive
468 multispectral imagery – and floristic composition, a trade-off between the floristic
469 significance of the clusters and the classification accuracy of the RS data should be taken into
470 account. As already pointed out (Thomas et al. 2003; Kumar & Sinha 2014; Martínez-López
471 et al. 2014), a solely floristic-based typology produced an inaccurate classification of remote
472 sensing data (~25 – 40 %). To address this issue, a common approach is to aggregate plant
473 communities into vegetation formations such as lawns, sedges, poor fens, bogs, shrubs and
474 woods (Thomas et al. 2003; Middleton et al. 2012); open dwarf shrub, sparse grassland, and
475 woody acacia shrub (Oldeland et al. 2010) or mangrove, pasture, dry grass, and salt-marsh
476 vegetation (Kumar & Sinha 2014). One of the two main advances of our study is to show that
477 hybrid distance in a multivariate space combining the PCA scores of spectral and floristic data
478 produced a “compromise” typology – identifying 9 grassland plant communities, each with a

479 similar physiognomy – that could be accurately mapped. Figure 6 clearly shows that –
480 compared to the floristic typology – the compromise typology strongly improved RS
481 classification by 36 points (from 26% to 62%) while preserving the homogeneous floristic
482 clusters (the average silhouette value decreased slightly from 0.26 to 0.21).

483 Besides, both plant communities and dominant species can be mapped from hyperspectral
484 imagery (Schmidtlein et al. 2007), LiDAR point clouds (Zlinszky et al. 2014) or TerraSAR-X
485 time series (Schuster et al. 2015), but their high cost limits their use. Therefore, one of the
486 main results of the method was to establish a correspondence between our vegetation units
487 and the French national reference for natural habitats (Bioret et al. 2013). In this study,
488 correspondences between clusters and syntaxonomy units were based on expert-based
489 assignments because the French phytosociological system is not yet stabilized. In the near
490 future, an improved version of the system will be available based on the VegFrance database,
491 which includes digital *relevés* (Bonis & Bouzillé 2012) and the use of numerical approaches
492 (Tichý et al. 2014).

493 Several improvements to the development of the typology can be suggested. It should be
494 recalled that spectral clusters (i.e. canopy reflectance) vary over time (Feilhauer et al. 2016),
495 as do floristic clusters. To transfer this approach to other sites, satellite images should be
496 acquired during the optimal period: from maximum development of herbaceous vegetation to
497 the beginning of mowing. This issue can also be addressed by analyzing annual satellite time
498 series to examine dynamics of the spectral response of vegetation over time (Schuster et al.
499 2015; Shoko & Mutanga 2017). Besides, the use of NMDS scaling would result in all of the
500 floristic variance being found on either two or three axes (Schmidtlein et al. 2007; Feilhauer
501 et al. 2014) compared with only 38% of the floristic variance, as observed in the PCA we used
502 in the present study. However, NMDS axes should be carefully interpreted as a function of the
503 stress value (Clarke 1993). Moreover, NMDS scaling may be influenced by rare species,

504 which may lead to incorrect interpretations (Legendre & Gallagher 2001). Indeed, preliminary
505 tests we performed on the dataset showed that PCA produced a clearer pattern than NMDS
506 due to two “outlier” *relevés* dominated by *Phragmites australis* and *Phalaris arundinacea*
507 species. The second issue is related to the definition of the number of clusters. In this study,
508 the reliability of the clusters was assessed with average silhouette value, the number of
509 diagnostic species and Hubert' C-indexes, usually used in vegetation science for
510 phytosociological classifications (Douda et al. 2016); however, the effectiveness of the
511 silhouette method is still an open question (Dengler et al. 2013). Otherwise, the set of field
512 data upon which the classification of the nine clusters is based consists of 213 plots. In the
513 near future, it will be useful to check this using more plots. In this regard, the national
514 vegetation data base is a promising tool (Bonis & Bouzillé 2012).

515 *4.2 Contribution of the fuzzy approach*

516 This study highlights that the integration of floristic and spectral uncertainty by using a fuzzy
517 approach increased the accuracy of a vegetation map by 17% (**Fig. 5**). The comprehensive
518 fuzzy approach we have developed includes: 1-the fuzzy classification of vegetation data, 2-
519 the fuzzy classification of remote sensing data and 3-the fuzzy accuracy assessment of the
520 resulting map. This approach can be used to consider both the floristic and spectral
521 uncertainty over the entire analysis, something that has been identified as an important
522 challenge of vegetation mapping (Rocchini 2014). When the comprehensive fuzzy approach
523 is not used, the remote-sensing data classification may be biased by an arbitrary expert-based
524 typology. Thus, it seems that the fuzzy approach is needed to map natural habitats,
525 specifically those in wetlands where subtle variations in topography and pasturage have a
526 fine-grained pattern, with progressive transitions between habitats (Dumont et al. 2012); in
527 the present study, 35% of *relevés* were not clearly assigned to a vegetation unit (Figure 3). As
528 a result, the uncertainty map (Figure 4) contains many uncertain pixels (in black), which can

529 be viewed initially as an obstacle to direct operational use. However, the uncertain pixels also
530 highlight target areas where additional field *relevés* are needed (Zlinszky & Kania 2016).
531 Before analysis, we ensured that *relevés* were floristically and spectrally homogeneous to
532 avoid ambiguities between ground data and remote sensing imagery. This common
533 preliminary step is essential to remove *relevés* with spurious spectral values, such as those
534 associated with the presence of clouds or cows (e.g. see Schmidtlein et al. (2007) or
535 Schmidtlein et al. (2012)). It was all the more necessary as spectral values of pixels were
536 averaged per *relevé*; in this sense, we consider that the fuzzy approach addresses uncertainty
537 between *relevés* but not within them. In our sampling design, only 7 of the 220 *relevés* were
538 discarded (< 2% of the total), because of spectral heterogeneity explained by shallow water on
539 part of the plot.

540 Many widely used supervised classifiers, such as support vector machine or random forest,
541 initially produce fuzzy outcomes before a final crisp classification. Several studies have
542 shown the contribution of such classifiers to fuzzy mapping of grassland habitats (Zlinszky et
543 al. 2014; Zlinszky & Kania 2016). In this study, we applied a noise-clustering classifier twice:
544 first as an unsupervised classifier to classify the pixels corresponding to vegetation *relevés*
545 and then as a supervised classifier to classify all the pixels in the image.

546 *4.3 The potential of cost-effective remote sensing data*

547 In this study, we opted for a cost-effective multispectral Pléiades satellite image (€1/km²) and
548 free national LiDAR-derived DTM rather than expensive RS data. The combined use of one
549 Pléiades image and a LiDAR-derived DTM resulted in a classification accuracy of 62%. In
550 accordance with (Feilhauer et al. 2013; Chasmer et al. 2014), we pointed out that LiDAR
551 DTM and near infrared spectra were important variables to discriminate natural habitats in
552 wetlands (Appendix S6). Specifically, the contribution of LiDAR DTM (+5% in overall

553 accuracy) corroborates previous studies highlighting the strong relationship between plant
554 community distribution and micro-topography in wetlands (Moeslund et al. 2011; Alexander
555 et al. 2016). It should be kept in mind, however, that this relationship can be biased locally by
556 water management such as intensive drainage for agriculture or, conversely, water retention
557 for conservation (Rapinel et al. 2018). Beyond 2-D LiDAR variables, many studies (Zlinszky
558 et al. 2014; Zlinszky et al. 2015) have also highlighted the contribution of 3-D variables such
559 as echo width, intensity response and surface roughness to accurately map grassland habitats
560 (overall accuracy 62-68%, kappa index 0.57-0.64). In this sense, combining multispectral
561 satellite imagery with point-cloud LiDAR data is a promising avenue for mapping plant
562 communities. The mapping accuracy may be slightly increased ($\pm 10\%$) with other cost-
563 effective multispectral satellite imagery such as RapidEye or SPOT-5, which feature
564 additional red edge and SWIR spectral bands, respectively, and which have been shown to be
565 relevant to accurately map wetland natural habitats (Davranche et al. 2010; Stenzel et al.
566 2014). Until now, accuracy greater than 85% could be reached only by using airborne
567 hyperspectral (Burai et al. 2015) ; hyperspatial resolution imagery from an unmanned aerial
568 vehicle (Kaneko & Nohara 2014) or full-waveform LiDAR data (Launeau et al. 2018) of
569 small sites covering several hectares. However, the new Sentinel time-series with a high
570 spatial resolution (10 m) seem promising to accurately map natural habitats, using Sentinel-1
571 SAR (Schmidt et al. 2017) or Sentinel-2 multispectral (Shoko & Mutanga 2017) sensors.
572 Such time-series satellite images, which are both free and cost-effective, are now available
573 and appear promising to accurately distinguish between plant communities in the near future.
574 Considering that the spectral response is partially linked to species composition as well as to
575 physiognomy, litter thickness, biomass and abiotic variables such as proportion of bare soil
576 and water content (Feilhauer et al. 2013), we hypothesized that a plant community may show
577 several spectral signatures. Our results confirmed this hypothesis as four clusters were

578 characterized by at least two spectral signatures. Specifically, cluster L2, corresponding to a
579 grazed hygrophilous plant community, has four spectral signatures. In wetland environments,
580 the presence of water in different proportions may explain this spectral variability from plant
581 community clusters, as highlighted in some Australian salt marshes (Kumar & Sinha 2014).
582 Future field campaigns with systematic measurements of the plant species composition
583 combined with biomass and abiotic variables could be used to explain the relationship
584 between the spectral responses and floristic composition, as done by Feilhauer et al. (2013).

585 4.4 A new way to monitor habitats for the UE Directive

586 Using RS data for application of the EU Habitats Directive has been emphasized for a decade
587 (Vanden Borre et al. 2011). Most RS studies, however, have focused on the Natura 2000
588 nomenclature (e.g. Alexandridis et al. 2009; Stenzel et al. 2014; Féret et al. 2015) rather than
589 on plant communities, which are the “elementary” units of biodiversity (Pott 2011). Rodwell
590 et al. (2018) and Bioret et al. (2017) recently urged clarifying the actual object of Natura 2000
591 reporting and the need to consider elementary habitats (i.e. plant communities). The approach
592 we developed, which was able to map 9 plant communities as “elementary” habitats, opens
593 avenues to do so. It should kept in mind that these elementary habitats form the basis of the
594 Natura 2000, CORINE and EUNIS nomenclatures, “though this involvement has been
595 complex and unclear” (Rodwell et al. 2018). Here, we used RS data to map 9 “elementary”
596 habitats that are included in the “thermo-Atlantic and sub-brackish meadows” Natura 2000
597 habitat, which encompasses diverse and even contrary environmental conditions caused by
598 environmental management such as flood duration (from less than 1 month for *Hordeo*
599 *secalini-Lolietum perennis* up to 4 months for *Eleocharito palustris-Oenanthetum fistulosae*)
600 and agricultural practices (grazing for *Carici divisae-Lolietum perennis* or mowing for *Junco*
601 *gerardi-Oenanthetum fistulosae*). From a structural perspective, each “elementary” habitat
602 that we mapped could be used as a surrogate of a species pool (Zlinszky et al. 2015) but also

603 of species richness, stand structural diversity or key species cover (Neumann et al. 2015;
604 Schmidt et al. 2017). From a functional perspective, these “elementary” habitats – which are
605 ecologically homogeneous units – could also provide insights into their corresponding
606 environmental conditions as well as their functional traits (e.g. seed mass), which are
607 indirectly detectable from RS data (Violle et al. 2011).

608 One challenge of applying the Habitats Directive is the field sampling effort. In accordance
609 with Zlinszky & Kania (2016), we believe that the fuzzy map with hue-preserving blending
610 provides a more realistic view of the complex spatial patterns of natural vegetation and
611 highlights transitional areas between habitats as well as uncertain areas (Fig. 4). This fuzzy
612 map provides useful and new guidelines to local managers for planning additional field
613 *relevés* and strengthening collaborations between remote sensing and ecologist communities
614 (Vanden Borre et al. 2011).

615 **Conclusion**

616 The comprehensive fuzzy procedure successfully mapped herbaceous plant communities at
617 the ecosystem scale using inexpensive remote sensing data. Floristic and spectral uncertainty
618 was considered in a fuzzy approach, resulting in the mapping of 9 herbaceous plant
619 communities with acceptable accuracy. As the natural habitats were characterized at the plant
620 community level, correspondence with functional properties of the species or with ecosystem
621 services can be easily inferred. These encouraging results open up new ways to meet the
622 requirements for monitoring the conservation status of natural habitats in the EU Habitats
623 Directive

624 **Acknowledgements**

625 We are grateful to the French Ministry of Ecology - CarHab program - for funding the
626 research (Contract No. 2100992719). The authors would like to thank the ISIS program of the

627 French Space Agency (CNES) and the French Geographical Institute (IGN) for providing the
628 Pléiades imagery and LiDAR data. We thank Johan Oszwald for preliminary discussions on
629 this project and methodological advice and Adam Kania for processing the hue-preserving
630 blending algorithm. We also thank Olivier Jambon, Valérie Gouesbet, Guillaume Bouger,
631 Pauline Herbert and Olivier Gore for their help in the field and all land owners and managers
632 who gave us access to their fields and provided useful discussions.

633 **References**

- 634 Adler-Golden, S.M., Matthew, M.W., Bernstein, L.S., Levine, R.Y., Berk, A., Richtsmeier, S.C., Acharya,
635 P.K., Anderson, G.P., Felde, J.W., Gardner, J.A., Hoke, M.L., Jeong, L.S., Pukall, B., Ratkowski,
636 A.J., & Burke, H.K. 1999. Atmospheric correction for shortwave spectral imagery based on
637 MODTRAN4. In pp. 61–69.
- 638 Alber, A., & Piégay, H. 2011. Spatial disaggregation and aggregation procedures for characterizing
639 fluvial features at the network-scale: Application to the Rhône basin (France).
640 *Geomorphology* 125: 343–360.
- 641 Alexander, C., Deák, B., & Heilmeyer, H. 2016. Micro-topography driven vegetation patterns in open
642 mosaic landscapes. *Ecological Indicators* 60: 906–920.
- 643 Alexandridis, T.K., Lazaridou, E., Tsirika, A., & Zalidis, G.C. 2009. Using Earth Observation to update a
644 Natura 2000 habitat map for a wetland in Greece. *Journal of Environmental Management* 90:
645 2243–2251.
- 646 Ali, I., Cawkwell, F., Dwyer, E., Barrett, B., & Green, S. 2016. Satellite remote sensing of grasslands:
647 from observation to management. *Journal of Plant Ecology* 9: 649–671.
- 648 Amiaud, B., Bouzillé, J.-B., Tournade, F., & Bonis, A. 1998. Spatial patterns of soil salinities in old
649 embanked marshlands in western France. *Wetlands* 18: 482–494.
- 650 Berg, C., Abdank, A., Isermann, M., Jansen, F., Timmermann, T., & Dengler, J. 2014. Red Lists and
651 conservation prioritization of plant communities – a methodological framework. *Applied*
652 *Vegetation Science* 17: 504–515.
- 653 Bezdek, J.C., Ehrlich, R., & Full, W. 1984. FCM: The fuzzy c-means clustering algorithm. *Computers &*
654 *Geosciences* 10: 191–203.
- 655 Binaghi, E., Brivio, P.A., Ghezzi, P., & Rampini, A. 1999. A fuzzy set-based accuracy assessment of soft
656 classification. *Pattern Recognition Letters* 20: 935–948.
- 657 Bioret, F., Capelo, J., & Pedrotti, F. 2017. À propos de la cartographie des habitats d'intérêt
658 communautaire de la Directive européenne Habitats FauneFlore 92/43/CE. *Documents*
659 *Phytosociologiques* 6: 447–451.

- 660 Bioret, F., Gaudillat, V., & Royer, J.M. 2013. The Prodrome of French vegetation: a national synsystem
661 for phytosociological knowledge and management issues. *Plant sociology* 50: 17–21.
- 662 Bivand, R., Keitt, T., & Rowlingson, B. 2015. *rgdal: Bindings for the Geospatial Data Abstraction*
663 *Library*.
- 664 Bonis, A., & Bouzillé, J. aB. 2012. The project VegFrance: Towards a national vegetation database for
665 France. *Plant Sociology* 49: 97a99.
- 666 Braun-Blanquet, J. 1932. Plant Sociology. The study of plant communities. *Plant sociology. The study*
667 *of plant communities. First ed.*
- 668 Burai, P., Deák, B., Valkó, O., & Tomor, T. 2015. Classification of Herbaceous Vegetation Using
669 Airborne Hyperspectral Imagery. *Remote Sensing* 7: 2046–2066.
- 670 Chasmer, L., Hopkinson, C., Veness, T., Quinton, W., & Baltzer, J. 2014. A decision-tree classification
671 for low-lying complex land cover types within the zone of discontinuous permafrost. *Remote*
672 *Sensing of Environment* 143: 73–84.
- 673 Chuang, J., Weiskopf, D., & Moller, T. 2009. Hue-Preserving Color Blending. *IEEE Transactions on*
674 *Visualization and Computer Graphics* 15: 1275–1282.
- 675 Chytrý, M., Tichý, L., Holt, J., & Botta-Dukát, Z. 2002. Determination of diagnostic species with
676 statistical fidelity measures. *Journal of Vegetation Science* 13: 79–90.
- 677 Clarke, K.R. 1993. Non-parametric multivariate analyses of changes in community structure. *Austral*
678 *ecology* 18: 117–143.
- 679 Corbane, C., Lang, S., Pipkins, K., Alleaume, S., Deshayes, M., García Millán, V.E., Strasser, T., Vanden
680 Borre, J., Toon, S., & Michael, F. 2015. Remote sensing for mapping natural habitats and their
681 conservation status – New opportunities and challenges. *International Journal of Applied*
682 *Earth Observation and Geoinformation* 37: 7–16.
- 683 Davranche, A., Lefebvre, G., & Poulin, B. 2010. Wetland monitoring using classification trees and
684 SPOT-5 seasonal time series. *Remote Sensing of Environment* 114: 552–562.
- 685 De Cáceres, M. 2016. Package ‘vegclust.’
- 686 De Cáceres, M., Chytrý, M., Agrillo, E., Attorre, F., Botta-Dukát, Z., Capelo, J., Czúcz, B., Dengler, J.,
687 Ewald, J., Faber-Langendoen, D., Feoli, E., Franklin, S.B., Gavilán, R., Gillet, F., Jansen, F.,
688 Jiménez-Alfaro, B., Krestov, P., Landucci, F., Lengyel, A., Loidi, J., Mucina, L., Peet, R.K.,
689 Roberts, D.W., Roleček, J., Schaminée, J.H.J., Schmidtlein, S., Theurillat, J.-P., Tichý, L.,
690 Walker, D.A., Wildi, O., Willner, W., Wiser, S.K., & Scheiner, S. 2015. A comparative
691 framework for broad-scale plot-based vegetation classification. *Applied Vegetation Science*
692 18: 543–560.
- 693 De Cáceres, M., Font, X., & Oliva, F. 2010. The management of vegetation classifications with fuzzy
694 clustering. *Journal of Vegetation Science* 21: 1138–1151.
- 695 Dengler, J. 2017. Phytosociology. In *International Encyclopedia of Geography*, pp. 1–6. American
696 Cancer Society.

- 697 Dengler, J., Bergmeier, E., Willner, W., & Chytrý, M. 2013. Towards a consistent classification of
698 European grasslands. *Applied Vegetation Science* 16: 518–520.
- 699 Dou, W., Ren, Y., Wu, Q., Ruan, S., Chen, Y., Bloyet, D., & Constans, J.-M. 2007. Fuzzy kappa for the
700 agreement measure of fuzzy classifications. *Neurocomputing* 70: 726–734.
- 701 Douda, J., Boublík, K., Slezák, M., Biurrun, I., Nociar, J., Havrdová, A., Doudová, J., Ačić, S., Brisse, H.,
702 Brunet, J., Chytrý, M., Claessens, H., Csiky, J., Didukh, Y., Dimopoulos, P., Dullinger, S.,
703 FitzPatrick, Ú., Guisan, A., Horchler, P.J., Hrivnák, R., Jandt, U., Kaçki, Z., Kevey, B., Landucci,
704 F., Lecomte, H., Lenoir, J., Paal, J., Paternoster, D., Pauli, H., Pielech, R., Rodwell, J.S.,
705 Roelandt, B., Svenning, J.-C., Šibík, J., Šilc, U., Škvorc, Ž., Tsiripidis, I., Tzonev, R.T.,
706 Wohlgemuth, T., & Zimmermann, N.E. 2016. Vegetation classification and biogeography of
707 European floodplain forests and alder carrs. *Applied Vegetation Science* 19: 147–163.
- 708 Dray, S., & Dufour, A.-B. 2007. The ade4 package: implementing the duality diagram for ecologists.
709 *Journal of statistical software* 22: 1–20.
- 710 Duff, T.J., Bell, T.L., & York, A. 2014. Recognising fuzzy vegetation pattern: the spatial prediction of
711 floristically defined fuzzy communities using species distribution modelling methods. *Journal*
712 *of Vegetation Science* 25: 323–337.
- 713 Dumont, B., Rossignol, N., Loucougaray, G., Carrère, P., Chadoeuf, J., Fleurance, G., Bonis, A.,
714 Farruggia, A., Gaucherand, S., Ginane, C., Louault, F., Marion, B., Mesléard, F., & Yavercovski,
715 N. 2012. When does grazing generate stable vegetation patterns in temperate pastures?
716 *Agriculture, Ecosystems & Environment* 153: 50–56.
- 717 Feilhauer, H., Dahlke, C., Doktor, D., Lausch, A., Schmidtlein, S., Schulz, G., & Stenzel, S. 2014.
718 Mapping the local variability of Natura 2000 habitats with remote sensing. *Applied*
719 *Vegetation Science* 17: 765–779.
- 720 Feilhauer, H., Somers, B., & van der Linden, S. 2016. Optical trait indicators for remote sensing of
721 plant species composition: Predictive power and seasonal variability. *Ecological Indicators*
- 722 Feilhauer, H., Thonfeld, F., Faude, U., He, K.S., Rocchini, D., & Schmidtlein, S. 2013. Assessing floristic
723 composition with multispectral sensors—A comparison based on monotemporal and
724 multiseasonal field spectra. *International Journal of Applied Earth Observation and*
725 *Geoinformation* 21: 218–229.
- 726 Féret, J.B., Corbane, C., & Alleaume, S. 2015. Detecting the Phenology and Discriminating
727 Mediterranean Natural Habitats With Multispectral Sensors #x2014;An Analysis Based on
728 Multiseasonal Field Spectra. *IEEE Journal of Selected Topics in Applied Earth Observations and*
729 *Remote Sensing* 8: 2294–2305.
- 730 Gargominy, O., Terceirie, S., Daszkiewicz, P., Régnier, C., Ramage, T., Dupont, P., & Poncet, L. 2012.
731 *TAXREF v5. 0, référentiel taxonomique pour la France: mise en œuvre et diffusion*. SPN, Paris.
- 732 Hennekens, S.M., & Schaminée, J.H.J. 2001. TURBOVEG, a comprehensive data base management
733 system for vegetation data. *Journal of Vegetation Science* 12: 589–591.
- 734 Hijmans, R.J. 2015. *raster: Geographic Data Analysis and Modeling*.
- 735 Hubert, L., & Arabie, P. 1985. Comparing partitions. *Journal of Classification* 2: 193–218.

- 736 Kaneko, K., & Nohara, S. 2014. Review of effective vegetation mapping using the UAV (Unmanned
737 Aerial Vehicle) method. *Journal of Geographic Information System* 6: 733.
- 738 Kumar, L., & Sinha, P. 2014. Mapping salt-marsh land-cover vegetation using high-spatial and
739 hyperspectral satellite data to assist wetland inventory. *GIScience & remote sensing* 51: 483–
740 497.
- 741 Lang, S., Mairota, P., Pernkopf, L., & Schioppa, E.P. 2015. Earth observation for habitat mapping and
742 biodiversity monitoring. *International Journal of Applied Earth Observation and*
743 *Geoinformation* 37: 1–6.
- 744 Launeau, P., Giraud, M., Ba, A., Moussaoui, S., Robin, M., Debaine, F., Lague, D., & Le Menn, E. 2018.
745 Full-Waveform LiDAR Pixel Analysis for Low-Growing Vegetation Mapping of Coastal
746 Foredunes in Western France. *Remote Sensing* 10: 669.
- 747 Lausch, A., Bannehr, L., Beckmann, M., Boehm, C., Feilhauer, H., Hacker, J., Heurich, M., Jung, A.,
748 Klenke, R., Neumann, C., & others. 2016. Linking Earth Observation and taxonomic, structural
749 and functional biodiversity: Local to ecosystem perspectives. *Ecological Indicators* 70: 317–
750 339.
- 751 Lavorel, S., Grigulis, K., Lamarque, P., Colace, M.-P., Garden, D., Girel, J., Pellet, G., & Douzet, R. 2011.
752 Using plant functional traits to understand the landscape distribution of multiple ecosystem
753 services. *Journal of Ecology* 99: 135–147.
- 754 Legendre, P., & Gallagher, E.D. 2001. Ecologically meaningful transformations for ordination of
755 species data. *Oecologia* 129: 271–280.
- 756 Lindsay, J., & Dhun, K. 2015. Modelling surface drainage patterns in altered landscapes using LiDAR.
757 *International Journal of Geographical Information Science* 29: 397–411.
- 758 Marion, B., Bonis, A., & Bouzillé, J.-B. 2010. How Much does Grazing-Induced Heterogeneity Impact
759 Plant Diversity in Wet Grasslands? *Ecoscience* 17: 229–239.
- 760 Martínez-López, J., Carreño, M.F., Palazón-Ferrando, J.A., Martínez-Fernández, J., & Esteve, M.A.
761 2014. Remote sensing of plant communities as a tool for assessing the condition of semiarid
762 Mediterranean saline wetlands in agricultural catchments. *International Journal of Applied*
763 *Earth Observation and Geoinformation* 26: 193–204.
- 764 Middleton, M., Närhi, P., Arkimaa, H., Hyvönen, E., Kuosmanen, V., Treitz, P., & Sutinen, R. 2012.
765 Ordination and hyperspectral remote sensing approach to classify peatland biotopes along
766 soil moisture and fertility gradients. *Remote Sensing of Environment* 124: 596–609.
- 767 Moeslund, J.E., Arge, L., Bøcher, P.K., Nygaard, B., & Svenning, J.-C. 2011. Geographically
768 Comprehensive Assessment of Salt-Meadow Vegetation-Elevation Relations Using LiDAR.
769 *Wetlands* 31: 471–482.
- 770 Mountrakis, G., Im, J., & Ogole, C. 2011. Support vector machines in remote sensing: A review. *ISPRS*
771 *Journal of Photogrammetry and Remote Sensing* 66: 247–259.
- 772 Neumann, C., Weiss, G., Schmidlein, S., Itzerott, S., Lausch, A., Doktor, D., & Brell, M. 2015. Gradient-
773 Based Assessment of Habitat Quality for Spectral Ecosystem Monitoring. *Remote Sensing* 7:
774 2871–2898.

- 775 Oksanen, J., Blanchet, F.G., Kindt, R., Legendre, P., Minchin, P.R., O'Hara, R.B., Simpson, G.L.,
776 Solymos, P., Stevens, M.H.H., & Wagner, H. 2015. *vegan: Community Ecology Package*.
- 777 Oldeland, J., Dorigo, W., Lieckfeld, L., Lucieer, A., & Jürgens, N. 2010. Combining vegetation indices,
778 constrained ordination and fuzzy classification for mapping semi-natural vegetation units
779 from hyperspectral imagery. *Remote Sensing of Environment* 114: 1155–1166.
- 780 Panem, C., Bignalet-Cazalet, F., & Baillarin, S. 2012. Pleiades-HR system products performance after
781 in-orbit commissioning phase. *ISPRS–International Archives of the Photogrammetry, Remote*
782 *Sensing and Spatial Information Sciences* 39: 567–572.
- 783 Peeters, A. 2009. Importance, evolution, environmental impact and future challenges of grasslands
784 and grassland-based systems in Europe. *Grassland Science* 55: 113–125.
- 785 Pott, R. 2011. Phytosociology: A modern geobotanical method. *Plant Biosystems - An International*
786 *Journal Dealing with all Aspects of Plant Biology* 145: 9–18.
- 787 Rapinel, S., Dusseux, P., Bouzillé, J.-B., Bonis, A., Lalanne, A., & Hubert-Moy, L. 2018. Structural and
788 functional mapping of geosigmeta in Atlantic coastal marshes (France) using a satellite time
789 series. *Plant Biosystems - An International Journal Dealing with all Aspects of Plant Biology*.
790 doi: 10.1080/11263504.2017.1418447
- 791 Rapinel, S., Hubert-Moy, L., & Clément, B. 2015. Combined use of LiDAR data and multispectral earth
792 observation imagery for wetland habitat mapping. *International Journal of Applied Earth*
793 *Observation and Geoinformation* 37: 56–64.
- 794 Rocchini, D. 2014. Fuzzy species distribution models: a way to represent plant communities spatially.
795 *Journal of Vegetation Science* 25: 317–318.
- 796 Rocchini, D., Boyd, D.S., Féret, J.-B., Foody, G.M., He, K.S., Lausch, A., Nagendra, H., Wegmann, M., &
797 Pettorelli, N. 2016. Satellite remote sensing to monitor species diversity: potential and
798 pitfalls. *Remote Sensing in Ecology and Conservation* 2: 25–36.
- 799 Rocchini, D., & Cade, B.S. 2008. Quantile Regression Applied to Spectral Distance Decay. *IEEE*
800 *Geoscience and Remote Sensing Letters* 5: 640–643.
- 801 Rocchini, D., Foody, G.M., Nagendra, H., Ricotta, C., Anand, M., He, K.S., Amici, V., Kleinschmit, B.,
802 Förster, M., Schmidlein, S., Feilhauer, H., Ghisla, A., Metz, M., & Neteler, M. 2013.
803 Uncertainty in ecosystem mapping by remote sensing. *Computers & Geosciences* 50: 128–
804 135.
- 805 Rodwell, J.S., Evans, D., & Schaminée, J.H.J. 2018. Phytosociological relationships in European Union
806 policy-related habitat classifications. *Rendiconti Lincei. Scienze Fisiche e Naturali*. doi:
807 10.1007/s12210-018-0690-y
- 808 Roelofsen, H.D., Kooistra, L., van Bodegom, P.M., Verrelst, J., Krol, J., & Witte, J.-P.M. 2014. Mapping
809 a priori defined plant associations using remotely sensed vegetation characteristics. *Remote*
810 *Sensing of Environment* 140: 639–651.
- 811 Roth, K.L., Roberts, D.A., Dennison, P.E., Peterson, S.H., & Alonzo, M. 2015. The impact of spatial
812 resolution on the classification of plant species and functional types within imaging
813 spectrometer data. *Remote Sensing of Environment* 171: 45–57.

- 814 Rousseuw, P.J. 1987. Silhouettes: A graphical aid to the interpretation and validation of cluster
815 analysis. *Journal of Computational and Applied Mathematics* 20: 53–65.
- 816 Schmidt, J., Fassnacht, F.E., Förster, M., & Schmidtlein, S. 2017. Synergetic use of Sentinel-1 and
817 Sentinel-2 for assessments of heathland conservation status. *Remote Sensing in Ecology and*
818 *Conservation*
- 819 Schmidt, T., Schuster, C., Kleinschmit, B., & Förster, M. 2014. Evaluating an Intra-Annual Time Series
820 for Grassland Classification #x2014;How Many Acquisitions and What Seasonal Origin Are
821 Optimal? *IEEE Journal of Selected Topics in Applied Earth Observations and Remote Sensing* 7:
822 3428–3439.
- 823 Schmidtlein, S., Feilhauer, H., & Bruelheide, H. 2012. Mapping plant strategy types using remote
824 sensing. *Journal of Vegetation Science* 23: 395–405.
- 825 Schmidtlein, S., Zimmermann, P., Schüpferling, R., & Weiß, C. 2007. Mapping the floristic continuum:
826 Ordination space position estimated from imaging spectroscopy. *Journal of Vegetation*
827 *Science* 18: 131–140.
- 828 Schuster, C., Schmidt, T., Conrad, C., Kleinschmit, B., & Förster, M. 2015. Grassland habitat mapping
829 by intra-annual time series analysis – Comparison of RapidEye and TerraSAR-X satellite data.
830 *International Journal of Applied Earth Observation and Geoinformation* 34: 25–34.
- 831 Shoko, C., & Mutanga, O. 2017. Seasonal discrimination of C3 and C4 grasses functional types: An
832 evaluation of the prospects of varying spectral configurations of new generation sensors.
833 *International Journal of Applied Earth Observation and Geoinformation* 62: 47–55.
- 834 Stenzel, S., Feilhauer, H., Mack, B., Metz, A., & Schmidtlein, S. 2014. Remote sensing of scattered
835 Natura 2000 habitats using a one-class classifier. *International Journal of Applied Earth*
836 *Observation and Geoinformation* 33: 211–217.
- 837 Stratford, C., Brewin, P., Acreman, M., & Mountford, O. 2015. A simple model to quantify the
838 potential trade-off between water level management for ecological benefit and flood risk.
839 *Ecohydrology & Hydrobiology* 15: 150–159.
- 840 Thomas, V., Treitz, P., Jelinski, D., Miller, J., Lafleur, P., & McCaughey, J.H. 2003. Image classification
841 of a northern peatland complex using spectral and plant community data. *Remote Sensing of*
842 *Environment* 84: 83–99.
- 843 Tichý, L., Chytrý, M., & Botta-Dukát, Z. 2014. Semi-supervised classification of vegetation: preserving
844 the good old units and searching for new ones. *Journal of Vegetation Science* 25: 1504–1512.
- 845 Vanden Borre, J., Paelinckx, D., Múcher, C.A., Kooistra, L., Haest, B., De Blust, G., & Schmidt, A.M.
846 2011. Integrating remote sensing in Natura 2000 habitat monitoring: Prospects on the way
847 forward. *Journal for Nature Conservation* 19: 116–125.
- 848 Violle, C., Bonis, A., Plantegenest, M., Cudennec, C., Damgaard, C., Marion, B., Le Cœur, D., &
849 Bouzillé, J.-B. 2011. Plant functional traits capture species richness variations along a flooding
850 gradient. *Oikos* 120: 389–398.
- 851 Wiser, S.K., & Cáceres, M. 2013. Updating vegetation classifications: an example with New Zealand’s
852 woody vegetation. *Journal of Vegetation Science* 24: 80–93.

- 853 Zadeh, L.A. 1965. Fuzzy sets. *Information and control* 8: 338–353.
- 854 Zlinszky, A., Deák, B., Kania, A., Schroiff, A., & Pfeifer, N. 2015. Mapping Natura 2000 Habitat
855 Conservation Status in a Pannonic Salt Steppe with Airborne Laser Scanning. *Remote Sensing*
856 7: 2991–3019.
- 857 Zlinszky, A., & Kania, A. 2016. Will it blend? Visualization and accuracy evaluation of highresolution
858 fuzzy vegetation maps. *International Archives of the Photogrammetry, Remote Sensing &*
859 *Spatial Information Sciences* 41:.
- 860 Zlinszky, A., Schroiff, A., Kania, A., Deák, B., Mücke, W., Vári, Á., Székely, B., & Pfeifer, N. 2014.
861 Categorizing Grassland Vegetation with Full-Waveform Airborne Laser Scanning: A Feasibility
862 Study for Detecting Natura 2000 Habitat Types. *Remote Sensing* 6: 8056–8087.
- 863

Supporting information

Appendix S1. Fuzzy accuracy assessment

Appendix S2. Dendrogram and silhouette plots

Appendix S3. Full synoptic table

Appendix S4. Reference and classified membership matrix

Appendix S5. Full map of the plant communities

Appendix S6. Importance of spectral bands on classification accuracy